Indian Journal of Pure & Applied Physics
Vol. 64, April 2026, pp. 398-408
DOI: 10.56042/ijpap.v64i4.26122

Investigation of Photo Sensitive Properties of Ferroelectric Stannous Chloride Dihydrate Doped Triglycine Sulphate ($SnCl_2.2H_2O$-TGS) Crystal by Pseudo Spin Lattice Coupled Mode (PLCM) Model

Ashish Nautiyal[a*], Subhash Singh[b] & Mayank Joshi[c]

[a]Department of Physics, Government Degree College, Rudraparyag, Uttarakhand 246171, India
[b]Department of Physics, Maulana Azad National Institute of Technology, Bhopal 462 003, India
[c]Department of Mathematics, H N B Garhwal University, Srinagar, Garhwal, Uttarakhand 246 174, India

Received: 2nd December 2025; accepted: 11th February 2026

A modified theoretical model based on a time, temperature dependent Green's function formalism has been constructed by integrating the Pseudo-Spin Lattice Coupled Mode (PLCM) approach with the Ising spin framework to investigate ferroelectric characteristics in stannous chloride dihydrate doped triglycine sulphate ($SnCl_2.2H_2O$-TGS) crystal. The formulation incorporates renormalized boundary condition for polarization, explicitly accounting for phonon anharmonicity up to the fourth order, together with coupling contributions from an externally applied electric field. This model has been utilized to analyze the second-order phase transition behaviour of $SnCl_2.2H_2O$ doped TGS, offering a detailed theoretical perspective on its ferroelectric phase stability. In addition, the work evaluates the photoactive performance parameters of the doped system, particularly emphasizing the photosensitivity figure of merit (M_1), high-current responsivity (M_2), vidicon suitability factor (M_3) and their corresponding ratios $\frac{M_2}{M_1}$, $\frac{M_3}{M_2}$ and $\frac{M_3}{M1}$ under both bias-free and externally biased field environments. The findings underscore that higher-order anharmonic lattice interactions and polarization-field coupling significantly contribute to the tunability and enhancement of the electromechanical and optoelectronic behaviour of stannous chloride dihydrate doped triglycine sulphate ($SnCl_2.2H_2O$-TGS) crystals, thereby demonstrating their potential for advanced ferroelectric and photosensitive device applications.

Keywords: Phonon anharmonic interaction, Electromechanical, Optoelectric

1 Introduction

Ferroelectric materials occupy a central position in condensed matter physics owing to their extensive utility across diverse technological domains, including computing systems, sensing devices, nanotechnology and even food-processing technologies. A wide range of ferroelectric crystals has been investigated over the years, such as triglycine sulphate (TGS), deuterated triglycine sulphate (DTGS), triglycine selenate (TGSe) and deuterated triglycine selenate (DTGSe). Among these, TGS has emerged as one of the most significant and thoroughly studied materials[1] in 1956. TGS exhibits a remarkably high value of spontaneous polarization, approaching approximately 10^{14} charges per square centimetre at its end face. The spontaneous polarization is oriented along the b-axis and is predominantly observed on the (010) crystallographic plane, making TGS an important model system for the study of ferroelectric behaviour (Fig. 1).

Triglycine sulphate (TGS) crystallizes in the monoclinic system with a 2/m symmetry at temperatures above the Curie point (Tc). When the temperature drops below Tc, the mirror symmetry is lost, and the structure transforms into a polar monoclinic point group. The molecular arrangement

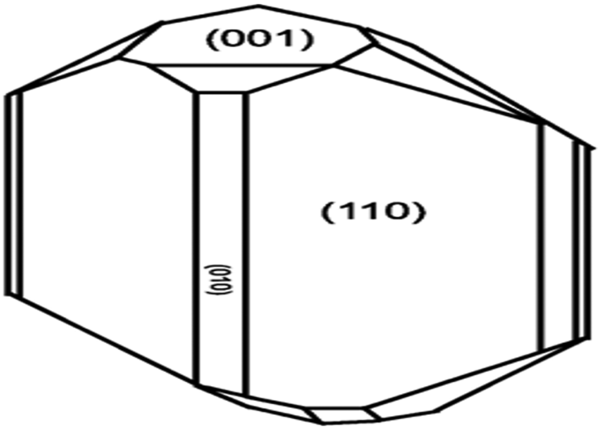

Fig. 1 — Crystal lattice faces[2]

---

[*]Corresponding author: E-mail: ashishnautiyal05@rediffmail.com

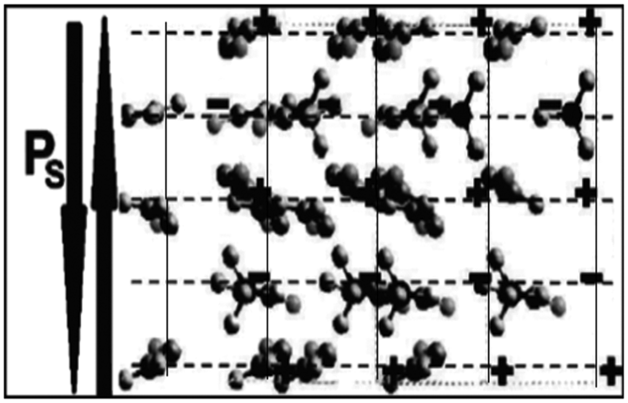

Fig. 2 — Polarization in triglycine sulphate crystal around the b-axis[3]

consists of three distinct glycine units: two of these (glycine groups II and III) adopt a nearly planar configuration, whereas the remaining unit (group I) exhibits a non-planar geometry. The planar glycine groups, II and III, occur as mirror-related counterparts and are oriented nearly perpendicular to the polar b-axis, contributing significantly to the development of spontaneous polarization in the ferroelectric phase. The spontaneous polarization in these crystals undergoes a reversible switching between the ferroelectric and Para electric phases, corresponding respectively to polar and non-polar states. This phase transition is accompanied by a pronounced increase in the dielectric permittivity (ε), which typically attains values on the order of 10^4–10^5 near the Curie temperature. The lattice dynamics of the crystal structure are highly sensitive to external stimuli, exhibiting measurable modifications under small variations in temperature, applied electric field, or photo-induced (electronic or thermal) perturbations. These dynamical responses can be characterized through the reorientation of dipoles, which align from 0° to 90° and subsequently from 90° to 180° under the influence of an external electric field, reflecting the microscopic mechanisms underlying polarization switching (Fig. 2).

Electrical discharge can arise at the interfaces between neighbouring ferroelectric domains with opposite polarization, as well as between such domains and external electrodes. Even in a nominally single-domain crystal, flashover may occur across different crystal surfaces. In triglycine sulphate (TGS), ionic defects and mobile electrons originating from the bulk contribute to charge screening over a characteristic timescale determined by the material's resistivity. These mobile carriers generate an additional space-charge polarization that significantly influences the dynamical response of ferroelectric crystals. While free carriers can partially neutralize each other, the bound surface charges associated with spontaneous polarization can only be screened not eliminated.

In triglycine sulphate (TGS) crystals, ion defects and mobile electrons originating from the bulk material contribute to the screening of spontaneous polarization over a characteristic time scale that is directly related to the electrical resistivity of the crystal. The movement of these charge carriers leads to the development of an additional space charge driven polarization, which exerts a strong influence on the dynamic response of the ferroelectric system. While the free carriers can neutralize oppositely charged counterparts, the intrinsic bound surface charges associated with spontaneous polarization cannot be neutralized, but only screened. Consequently, a dense accumulation of compensating charge forms at the crystal surface, and the domain structures become distinguishable under these conditions. The surface screening charges effectively isolate the external environment from the inherent dipole moment of the TGS crystal, resulting in an external electric field that is typically transient and significantly lower in magnitude compared with the expected theoretical value[4-6].

Due to these screening processes, a dense distribution of compensating charge accumulates on the major surfaces of TGS crystals, and the formation or stabilization of ferroelectric domains may occur concurrently. The screened surface charge effectively isolates the crystal's spontaneous polarization (dipole moment) from the external environment. As a result, the electric fields generated by the spontaneous polarization appear only briefly and with amplitudes substantially lower than the theoretical values predicted for an unscreened surface. The dielectric behaviour of stannous chloride dihydrate doped triglycine sulphate ($SnCl_2.2H_2O$-TGS) crystals reported[7] has provided valuable insight into the influence of dopants on ferroelectric response. Building upon this foundation, the present work extends the investigation toward the evaluation of vidicon constants and photoelectric sensitivity, thereby offering a broader understanding of the optoelectronic characteristics of TGS doped with stannous chloride dihydrate.

Thermal analysis confirmed that the introduction of doped does not induce any noticeable alteration in the intrinsic thermal stability of pure TGS. Furthermore, a detailed examination of the dielectric response indicated a significant improvement in dielectric permittivity as a consequence of doping. A measurable shift in the Curie transition temperature was also proposed, suggesting that doping plays a notable role in modifying the ferroelectric characteristics of TGS crystals[8]. It is noticeable that enhancement in the Curie transition temperature upon doping, demonstrating that the presence of the doping effectively alters the dielectric nature of TGS in pure and doped[9].

The central aim of this study is to identify the conditions under which photoelectric or photo thermal excitation can be detected in TGS-type ferroelectrics. The most favourable circumstances are expected during rapid polarization switching or during swift passage through the ferroelectric Para electric phase boundary, driven by an externally applied electric field pulse or a sudden mechanical pressure impulse. In general, ferroelectric phase transitions proceed through three characteristic stages and can be influenced by temperature variations, photoelectric or photo thermal excitation, and applied electric fields. Understanding these coupled effects is essential for elucidating the phase transition mechanisms and dynamic behaviour of hydrogen bonded ferroelectric crystals. In recent years, material optimization through selective doping has emerged as an effective route to enhance detector performance and operational stability. Dye-doped, rare-earth-doped, and the metal-ion-doped TGS crystals have shown marked improvements in pyroelectric figures of merit, dielectric stability, and the mechanical hardness, which are essential for reliable IR detection (M_1)[10,11]. Enhanced IR-induced output voltages and increased photosensitivity values have also been reported, indicating improved responsively and signal-to-noise ratio critical for high current response applications (M_2)[12,13]. Advanced growth approaches, including millimetre-wave irradiation and controlled solution growth techniques have further contributed to improved crystal quality and reduced defect density.

Although experimental investigations on $SnCl_2.2H_2O$-doped TGS crystals have been limited in the last decade, theoretical studies suggest that Sn^{2+} incorporation modifies hydrogen bonding networks and lattice dynamics, influencing dielectric relaxation and phonon behavior[14]. Such changes are expected to enhance charge generation efficiency under IR excitation. Furthermore, recent composite systems such as graphene-modified TGS crystals exhibit enhanced photothermal conversion and current output, reinforcing the potential of doped TGS materials for next-generation vidicon imaging and thermal camera systems (M_3). Overall, doped TGS crystals remain promising materials for advanced IR detection technologies with improved responsivity and device reliability.

Triglycine sulphate (TGS) and its doped variants continue to attract significant research attention due to their excellent pyroelectric and ferroelectric properties, making them suitable for M_1 – infrared (IR) detection, M_2–high current responsivity devices, and M_3 – vidicon and thermal imaging applications. The presence of spontaneous polarization along the crystallographic *b*-axis, together with a high pyroelectric coefficient and low dielectric loss, enables efficient thermal-to-electrical energy conversion in uncooled IR detectors. These intrinsic advantages have supported the long-standing use of TGS in thermal sensors and imaging elements.

2 Crystal Polarisation

The switching time of the polarization vector is strongly influenced by temperature, the magnitude of the applied direct-current electric field, and the several additional material- and defect-related factors, as originally reported[15]. For a pre-poled sample exhibiting two successive phase transitions, as discussed[16], the presence of space-charge layers at the crystal surface generates a substantial internal electric field oriented normal to the surface. When an external electric field is applied in a direction opposite to the intrinsic polarization, each antiparallel domain begins to expand, accompanied by lateral domain-wall motion. A rapid change in the polarization magnitude under these conditions can serve as a source of electron emission.

The largest surface charge densities are expected to arise from the combined action of polarization reversal and the release of trapped space charges induced by pulsed laser illumination. This photoelectric process produces electron emission, as demonstrated[17], suggesting that ferroelectric materials may serve as promising alternatives to conventional photocathodes. The importance is the ability to switch the polarization vector in such a way that electron emission occurs from the illuminated surface, thereby enhancing the overall emission efficiency. To enable this effect, the use of semitransparent electrodes facilitating both polarization reversal and efficient surface illumination has been recommended[18].

3 Calculation

The Hamiltonian H consists of a single particle part H_1 (i) and interaction part H_2 (i, j)

$$H = \sum_{i} H_1(i) + \sum_{i<j} H_2(i,j) , \qquad \text{... (1)}$$

In the representation in which the single particle Hamiltonian H_1 (i) is diagonal one gets

$$H_1 (i) = \sum_{\alpha} E_\alpha a^{i}{}_{\alpha +} a^{i}{}_{\alpha} \qquad \text{… (2)}$$

and

$$H_2 (i,j) = \sum_{\alpha\beta\gamma\delta} v^{ij}_{\alpha\beta}\, a^{i}_{\alpha}\, a^{i+}_{\beta}\, a^{j+}_{\gamma}\, a^{j}_{\delta} \qquad \text{… (3)}$$

where the operators $a^{i+}{}_{\propto}$ and $a^{i}{}_{\propto}$ are Fermi or Bose creation and annihilation operators for a proton or a deuteron respectively at site *i* in the single particle quantum state ∝. Since there is always only one Hydrogen nucleus in each hydrogen bond, the statistics are independent of the Fermi or Bose character of operators. The matrix element v_{ij} represents a general interaction between the ith and jth hydrogen bond which depends not only on the distance between the positions of *i* and j but also on their quantum states. The ground state of a single hydrogen in a double well is a doublet, and if higher excited states are neglected, the single-particle quantum numbers α, β, γ, and δ can take only two values, labeled + and –.

The corresponding Eigen functions

$$\psi_+ = \frac{1}{\sqrt{2}} (\psi_L + \psi_R) \qquad \text{… (4)}$$

$$\psi_- = \frac{1}{\sqrt{2}} (\psi_L - \psi_R) \qquad \text{… (5)}$$

which are the symmetric and antisymmetric linear combinations of wave functions localized in the left (ψ_L) and in right (ψ_R) equilibrium site.

The condition is that there is one and only one hydrogen atom in each bond is now expressed as

$$a^{i}_{+} a^{i}_{+} + a^{i+} a^{i}\_ = 1, \qquad \text{… (6)}$$

Using the above restrictions, one can now express the products of the creation and annihilation operators for a hydrogen in a given hydrogen bond with fictitious spin ½ operators

$$S^{x}_{i} = \frac{1}{2}\left(a^{i+}_{+} a^{i}_{+} - a^{i+}_{+} a^{i}_{-}\right), \qquad \text{… (7)}$$

$$S^{y}_{i} = \frac{1}{2}\left(a^{i+}_{+} a^{i}_{-} - a^{i+}_{-} a^{i}_{+}\right), \qquad \text{… (8)}$$

$$S^{z}_{i} = \frac{1}{2}\left(a^{i+}_{+} a^{i}_{-} - a^{i+}_{-} a^{i}_{+}\right), \qquad \text{… (9)}$$

which indeed obey the well-known commutation relations for spin operators

$$\left[S^{x}_{i}, S^{y}_{j}\right] = i\delta_{ij} S^{z}_{i} , \qquad \text{… (10)}$$

$$\left[S^{y}_{i}, S^{z}_{j}\right] = i\delta_{ij} S^{x}_{i} , \qquad \text{… (11)}$$

$$\left[S^{z}_{i}, S^{x}_{j}\right] = i\delta_{ij} S^{y}_{i} , \qquad \text{… (12)}$$

The operators $a+_\alpha$ and a_α are given as

$$a^{i}_{+} = \frac{1}{\sqrt{2}}\left(a^{i}_{L} + a^{i}_{R}\right), \qquad \text{… (13)}$$

$$a^{i+}_{+} = \frac{1}{\sqrt{2}}\left(a^{i+}_{L} + a^{i+}_{R}\right), \qquad \text{… (14)}$$

$$a^{i}_{-} = \frac{1}{\sqrt{2}}\left(a^{i}_{L} - a^{i}_{R}\right), \qquad \text{… (15)}$$

$$a^{i+}_{-} = \frac{1}{\sqrt{2}}\left(a^{i+}_{L} - a^{i+}_{R}\right), \qquad \text{… (16)}$$

Using Eqs. (9) and (13) to (16) one gets

$$S^{x}_{i} = \frac{1}{2}\left(a^{i+}_{L} a^{i}_{R} + a^{i+}_{R} a^{i}_{L}\right), \qquad \text{… (17)}$$

$$S^{y}_{i} = \frac{1}{2}\left(a^{i+}_{L} a^{i}_{R} - a^{i+}_{R} a^{i}_{L}\right), \qquad \text{… (18)}$$

$$S^{z}_{i} = \frac{1}{2}\left(a^{i+}_{L} a^{i+}_{L} - a^{i+}_{R} a^{i}_{R}\right), \qquad \text{… (19)}$$

Introducing the above spin operators into Eqs. (2) and (3) one gets

$$H = -\Omega \sum_{i} S^{x}_{i} - \frac{1}{2}\sum_{i,j} J_{ij} S^{z}_{i} S^{z}_{j} - \frac{1}{2}\sum_{i,j} B_{ij} S^{x}_{i} S^{x}_{j} \qquad \text{… (20)}$$

Where

$$\Omega = \left[E_- - E_+ + \sum_j \left(\upsilon^{ij}_{----} - \upsilon^{ij}_{++++} \right) \right],$$

$$\approx \left(E_- - E_+ \right), \qquad \ldots (21)$$

$$J_{ij} = -4\upsilon^{ij}_{+-+-}, \qquad \ldots (22)$$

And

$$B_{ij} = 2\upsilon^{ij}_{++-} - \upsilon^{ij}_{++++} - \upsilon^{ij}_{----} \qquad \ldots (23)$$

The terms like $S^x{}_i$, $S_j{}^z$ vanish for symmetry reasons as the Hamiltonian has to be invariant with respect to the exchange $S_i^z \rightarrow S_j^z$. It can be shown that B_{ij} $S^x{}_i$ $S^x{}_j$ term is small compared to Ω S^x term and can be neglected.

The tunneling integral frequency Ω is approximately equal to $\Omega \approx S\gamma_{OH}$ where γ_{OH} is the stretching frequency of an O-H...O hydrogen bonded proton and the overlap integral S is the order of 10^{-1} to 10^{-2} S and hence Ω strongly depends on the mass of the tunneling particle and on the width of the potential barrier separating the two equilibrium sites. The coefficient B in Eq. (23) representing effect of the tunneling motion of the one proton on the tunneling motion of another is of the order of $|B| \approx S^2\gamma_{OH}$ and can hence be safely neglected. The interaction constant J_{ij} represents relatively large terms but independent of S.

In view of the time dependence of Hamiltonian H, the expectation values of spin variables is also depend on time and designated by $\langle S_i(t) \rangle$. The time dependent molecular field $H_i(t)$ will therefore be given as $H_i(t) = -\delta\langle H \rangle / \delta\langle S_i \rangle t$, which is equivalent to the classical free precession of the psendospin around instantaneous value of molecular field at a given site.

The pressure dependence data[19,20] which showed strong pressure dependences of transition temperature, dielectric constant etc. in hidrogen bonded order-disorder ferroelectric type crystals. Therefore, the inclusion[21] of pseudospin-lattice coupling term in the pseudospin model.

$$H_{pl} = \frac{1}{4}\sum_k \omega_k (A_k^+ A_k + B_k^+ B_k) - \sum_{ik} V_{ik} S_i^z A_k \qquad \ldots (24)$$

where, V_{ik} is the pseudospin-lattice interaction constant. In Eq. (24) A_k and B_k are phonon operators corresponding to normal coordinates and the conjugate moment, ω_k is phonon harmonic frequency.

3.1 A Two Sub Lattice Pseudospin Coupled Mode

Raman spectroscopic data and dielectric results show that very small value of tunneling frequency ($\approx$ 0.10 cm^{-1}) occurs in hydrogen bonded order-diorder triglycine sulphate crystal in contrast to hydrogen bond ferroelectric crystal ($\approx$ 82 cm^{-1}). However large isotope effects on T_c and C occur in triglycine sulphate crystal. Dielectric properties, T_c and C of triglycine sulphate crystal are not greatly affected by deuterations showing that tunneling effect might not be very large in triglycine sulphate crystal. Due to this difference a pseudospin lattice coupled mode framework with two sublattices has been used for triglycine sulphate crystal. A two-sublattice pseudospin model is suggested for hydrogen bonded ferroelectric triglycine sulphate crystal[22-24].

Each of the N unit cells has four protons in which two are on H-bonds axis and two on bonds parallel to b-axis. Each proton is imagined to sit in one of two potential wells, through which it can tunnel. In this double well potential system one well is associated with a (+) and other with a (-) contribution to the polarization of the lattice, taken along +z. One describes the configuration of two protonic (a-orientation) groups by the eigen values ±½ of the operators $S^z_{2\alpha}\left(\alpha = 1,\ldots,2N\right)$, while the second groups are represented by $S^z_{1\alpha}$. The total lattice polarization is proportional to $\langle S^z_1 \rangle + \langle S^z_2 \rangle$. In fact, the protons in the polar phase fall into two nonequivalent groups having respective H-bonds.

The model Hamiltonian, that is, a two-sublattice pseudospin–lattice-coupled mode model considering both interchain and intrachain interactions, can be written for a hydrogen-bonded order–disorder type crystal as

$$\begin{aligned} H = & -2\Omega\sum_j \left(S^x_{1j} + S^x_{2j}\right) \\ & -\sum_{ij}\left[J_{ij}\left(S^z_{1j}S^z_{1j} + S^z_{2j}S^z_{2j}\right) + K_{ij}S^z_{1j}S^z_{2j}\right] \\ & -\sum_{ik} V_{ik}\left(S^z_{1j}A^+_k + S^z_{2j}A_k\right) \end{aligned} \qquad \ldots (25)$$

where S_α^m is the mth component of the pseudospin variable, $\vec{S}_\alpha(\alpha=1,2),\Omega$ is proton tunnelling frequency, and J_{ij} and K_{ij} describe, respectively, the proton coupling within a given chain and that between the protons of the two neighboring chains, denoted by 1 and 2.

3.2 Phonon Non-harmonic Interactions

The present study also considers the third-and the fourth-order phonon non-harmonic interaction terms[25-31] in the pseudospin-lattice coupled mode model[32]. The Hamiltonian of the non-harmonic crystal containing N unit cells with n atoms per-unit cell in the second quantized form inclusive of third and fourth-order non-harmonic interaction is expressed as H_{anh} =

$$\sum_{k_1k_2k_3} V^{(3)}(k_1k_2k_3)A_{k_1}A_{k_2}A_{k_3} + \sum_{k_1k_2k_3k_4} V^{(4)}(k_1k_2k_3k_4)A_{k_1}A_{k_2}A_{k_3}A_{k_4} \qquad \ldots (26)$$

Where the coefficients $V^{(3)}$ and $V^{(4)}$ are Fourier transforms of the third and fourth-order atomic force constants defined. They are completely symmetric in the indices k and are given by

$$V^{(3)}(k_1k_2k_3) = \frac{1}{6x2^{3/2}N^{1/2}}\frac{\hbar^{1/2}}{(\omega_{k_1}\omega_{k_2}\omega_{k_3})^{1/2}} \times \phi(k_1,k_2,k_3)\Delta(k_1+k_2+k_3) \qquad \ldots (27)$$

And

$$V^{(4)}(k_1,k_2,k_3,k_4) = \frac{1}{2^2\times 24N}\frac{\hbar^{1/2}}{(\omega_{k_1}\omega_{k_2}\omega_3\omega_{k_4})^{1/2}} \times\phi(k_1,k_2,k_3,k_4)\,\Delta(k_1+k_2+k_3+k_4) \qquad \ldots (28)$$

With

$$\phi(k_1,k_2,k_3,) = \sum_{i,j,k}\frac{\phi_{ijk}}{M^{3/2}}\vec{e}(k_1)\vec{e}(k_2)\vec{e}(k_3)\ \mathrm{X}\exp\lfloor i(k_1R_i+k_2R_j+k_3R_k)\rfloor, \qquad \ldots (29)$$

$$\phi(k_1,k_2,k_3,k_4) = \sum_{i,j,k}\frac{\phi_{ijkl}}{M^2}\vec{e}(k_1)\vec{e}(k_2)\vec{e}(k_3)\vec{e}(k_4)\ X\exp\lfloor i(k_1R_i+k_2R_j+k_3R_k+k_4R_l)\rfloor, \qquad \ldots (30)$$

where ϕ_{ijk} and ϕ_{ijkl} are the third and fourth-order force constants of the crystal and $\Delta(\vec{k})=1$ if $\vec{k}=0$ or a reciprocal lattice vector and zero otherwise. Here, N is the number of atoms, each having mass M, in a Bravais lattice.

3.3 Electric Field Effect

The external electric field term is added as

$$H_{elec} = -2\mu E\sum_i(S_{1i}^z+S_{2i}^z) \qquad \ldots (31)$$

where $E=E_{in}+E_{ex}$.In which $E_{in}$is the electric field due to $Sn^{2+}$and Cl^{2-} ions in the doped system. For the $SnCl_2.2H_2O$ doped triglycine sulphate (TGS) crystal, we employ an extended two-sublattice pseudospin lattice coupled mode framework, originally proposed in earlier studies, and further generalize it by incorporating third, fourth-order phonon anharmonic interaction, and dopant interation potential terms. In addition, the model is augmented with an external electric-field contribution. The resulting Hamiltonian can be formally expressed as:

$$\begin{aligned}
H = {} & -2\Omega\sum_i(S_{1i}^x+S_{2i}^x) - \sum_{ij}J_{ij}\lfloor(S_{1i}^zS_{2i}^z)+(S_{2i}^zS_{2i}^z)\rfloor \\
& -\sum_{ij}K_{ij}(S_{1i}^zS_{2i}^z) - 2\mu E\sum_i(S_{1i}^z+S_{2i}^z) \\
& +\frac{1}{4}\sum_k\omega_k(A_kA_k^+ + B_kB_k^+) - \sum_{ik}V_{ik}S_{1i}^zA_k - \sum_{ik}V_{ik}S_{2i}^zA_k^+ \\
& + \sum_{k_1k_2k_3}V^{(3)}(k_1,k_2,k_3)\,A_{k_1}A_{k_2}A_{k_3} \\
& + \sum_{k_1k_2k_3k_4}V^{(4)}(k_1,k_2,k_3,k_4)\,A_{k_1}A_{k_2}A_{k_3}A_{k_4} \\
& + \sum V(SnCl_2 - Interactions),
\end{aligned} \qquad \ldots (32)$$

In Eq. (32), Ω represents the proton-tunneling frequency, while S^z and S^x denote the components of the pseudospin variable associated with the two-sublattice system. The parameters J_{ij} and K_{ij} correspond to the intra-sublattice and inter-sublattice interaction strengths, respectively. The quantity μ refers to the dipole moment of the O–H⋯O hydrogen bond, and E is the externally applied electric field. The term V denotes the spin–lattice interaction potential, whereas A_k and B_k represent the canonical position and momentum operators of the lattice mode *k*. The frequency ω_k describes the harmonic phonon mode, and V^3 and V^4 are the third and fourth-order anharmonic force constants, respectively, which characterize higher-order lattice interactions.

The motion of a particle of mass *m*, constrained to move along the *x*-axis with an associated wave function Ψ(x, t), is governed by the time-dependent Schrödinger equation. This framework enables the evaluation of quantum states and dynamical behavior relevant to the coupled pseudospin–phonon model of triglycine sulphate. $\frac{\hbar^2}{2m}\frac{\partial^2\psi}{\partial x}+i\hbar\frac{\partial\psi}{\partial t}=V\psi$ This equation is formally analogous to Newton's second law F=ma, as it governs the evolution of a particle under the influence of a potential, though within the framework of quantum mechanics. In this formalism, Ψ(x,t) represents the wave function describing the particle's state at position x and time t. According to the Born statistical interpretation, the quantity $|\Psi(x,t)|^2$provides the probability density for locating the particle at a given position and time. By applying this interpretation, the time-dependent Schrödinger equation stated above can be solved under the prescribed boundary conditions to obtain physically meaningful eigenvalues and eigenfunctions relevant to the system under investigation at

$$\tan k_{1a}=-\frac{k_1}{k_2}=-\sqrt{\frac{E-V_0}{-E}}$$

3.4 Green's Function, Pseudospin, and Photosensitive Variables

The Green's function

$$G_{ij}(t-t')=\left\langle\left\langle S^z_{1i}(t);S^z_{1j}(t')\right\rangle\right\rangle$$
$$=-i\theta(t-t')\left\langle\left[S^z_{1i}(t);S^z_{1j}(t')\right]\right\rangle \quad \dots (33)$$

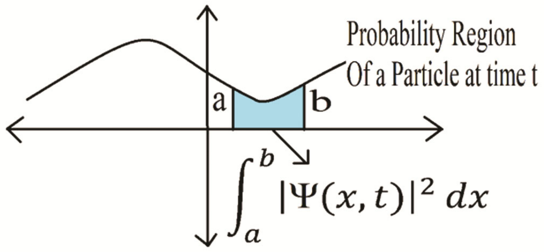

Fig. 3 — Expectation value of Eigen value of the crystal

In this expression, the function Θ(t−t′) represents the Heaviside step function, which evaluates to zero for t<t′ and to unity for t>t′. The angular brackets<⋯> denote an ensemble average taken over the grand canonical ensemble.

The spontaneous polarization in a $SnCl_2.2H_2O$-TGS crystal can be expressed as $P_S = 2N\mu < S^Z >$, where N is the number of dipoles, μ is the dipole moment, and $< S^Z >$ denotes the ensemble-averaged pseudospin component along the z-axis. In the ferroelectric phase ($T<T_C$), the two pseudospin components oriented along the z-direction do not cancel each other, and therefore their sum remains finite, $S_1^z+S_2^z\neq 0$, $S_1^z\neq S_2^z$. This non-zero net pseudospin alignment gives rise to a finite spontaneous polarization below the Curie temperature. Above the Curie temperature ($T>T_C$), thermal fluctuations dominate the dipolar ordering, leading to complete cancellation of the pseudospin contributions. Consequently, the total spontaneous polarization vanishes in the paraelectric phase, $S_1^z+S_2^z=0$, For stannous chloride dihydrate doped TGS, the behaviour of the pseudospin components near the phase transition exhibits characteristic features of a second-order ferroelectric–paraelectric transformation. In the ferroelectric region, the individual pseudospin components along the z-direction, S_1^z and S_2^z remain positive and finite, indicating the persistence of local dipolar alignment within the crystal lattice. However, as the system approaches the Curie temperature, the macroscopic spontaneous polarization P_s progressively decreases and tends toward zero, although it does not vanish abruptly. This continuous reduction of P_s reflects the nature of a second-order phase transition, where long-range order diminishes smoothly despite the local pseudospin components maintaining nonzero values close to the transition point. $< S^x >= \frac{\Omega}{\tilde{\Omega}}\tanh(\frac{\beta\tilde{\Omega}}{2})$,

$< S^y >= 0$

$$< S^z >= \frac{(J_0 < S^Z > + J_0{}' < S^Z >^3)}{2\tilde{\Omega}} \tanh(\frac{\beta\tilde{\Omega}}{2})$$

These pseudospin solutions are subsequently inserted into the corresponding eigenvalue equations, enabling the derivation of several key physical relations. From these solutions, expressions for the dielectric permittivity, microwave absorption characteristics, and the photo-sensitivity figures of merit are obtained, providing deeper insight into the electrodynamic and photoresponsive behaviour of the crystal system.

Appropriate boundary conditions are imposed to ensure the physical consistency of the pseudospin–lattice coupled mode model. Far from surfaces and impurity sites, the system is assumed to recover bulk ferroelectric behavior, with pseudospin expectation values approaching their bulk averages, consistent with the standard treatment of order–disorder ferroelectrics. Within the Green's function formalism, physically acceptable solutions are obtained by requiring that the pseudospin and phonon Green's functions vanish asymptotically at large spatial separations, ensuring the stability of long-wavelength collective modes. The presence of surfaces and dopant ions is accounted for through site-dependent exchange interactions and internal fields, reflecting local symmetry breaking and disorder effects commonly observed in doped hydrogen-bonded ferroelectrics. For the lattice degrees of freedom, mechanically free boundary conditions are assumed, as widely adopted in pseudospin phonon coupled models.

Within the PLCM framework, the polarization in SnCl$_2$.2H$_2$O-doped triglycine sulphate is subjected to electrostatic and mechanical boundary conditions such that the spatial derivative of polarization vanishes at the crystal surfaces, i.e., $\partial P/\partial z=0$ at $z = 0$. The associated pseudospin order parameters satisfy reduced surface values, while the coupled lattice displacement obeys rigid boundary conditions. Under external biasing, these boundary constraints are modified through the induced depolarization field, leading to enhanced polarization response near the phase transition.

Thus, the dielectric permittivity emerges as a complex quantity, comprising both real and imaginary components.

$$\varepsilon = \varepsilon' \pm i\varepsilon'' \qquad \ldots (34)$$

Where ε'=real and ε''=imaginary part of permittivity. Therefore, magnitude of this complex number will be

$$\varepsilon = \sqrt{(\varepsilon'^2 + \varepsilon''^2)} \qquad \ldots (35)$$

and dielectric loss

$$\tan \delta = \frac{\in''}{\in'} \qquad \ldots (36)$$

Solved equations,

$$\varepsilon' = \sqrt{(\frac{\varepsilon^2}{1+\tan^2\delta})} \text{ and, } \varepsilon'' = \sqrt{\frac{\varepsilon^2 \tan^2\delta}{1+\tan^2\delta}} \qquad \ldots (37)$$

in InfraRed detection the figure of merit can be written as:

$$M_1 = \frac{\rho}{\varepsilon'}$$

High current responsivity ... (38)

$$M_2 = \frac{\rho}{\sqrt{\varepsilon''}}$$

And vidicons application ... (39)

$$M_3 = \frac{\rho}{\sqrt{\varepsilon'}} \qquad \ldots (40)$$

Then relative figure of merits will be

$$\frac{M_2}{M_1} = \sqrt{\varepsilon''} \qquad \ldots (41)$$

$$\frac{M_3}{M_2} = \sqrt{\frac{\varepsilon''}{\varepsilon'}} \qquad \ldots (42)$$

$$\frac{M_3}{M1} = \frac{\varepsilon''}{\sqrt{\varepsilon'}} \qquad \ldots (43)$$

4 Results

The calculated values of infrared responsivity, high-current responsivity, and vidicon sensitivity for the SnCl$_2$.2H$_2$O-TGS crystal system using Tables 1 and 2 under investigation are presented in Figs. 4, 5 and 6, respectively.

5 Discussion

The present findings indicate that, although our understanding remains at an early stage, ferroelectric materials hold significant promise as photo thermal

Table 1 — Model values of physical parameters for TGS crystal

Sample	*A* (cm^{-1})	*J* (cm^{-1})	*V$_o$* (cm^{-1})	*ħω* (cm^{-1})	*N$_\mu$* (μC/cm^2)	*Ω* (cm^{-1})	*T$_c$* (^0C)	*C* (^0C)
TGS	10.20	340	10	0.59	2.22(323K)	0.1	49.1	3007

Table 2 — Pseudospin value of tunneling proton

Tem.	S_1^X	S_2^X	S_1^Z	S_2^Z
310	0.018	-0.017	0.15	-0.14
314	0.015	-0.014	0.14	-0.13
318	0.011	-0.010	0.12	-0.11
322	0.008	-0.007	0.11	-0.10
325	0.002	-0.002	0.09	-0.09
328	0.001	-0.001	0.10	-0.10
334	0.001	-0.001	0.11	-0.11
338	0.001	-0.001	0.12	-0.111
342	0.001	-0.001	0.13	-0.12
346	0.001	-0.001	0.14	-0.13

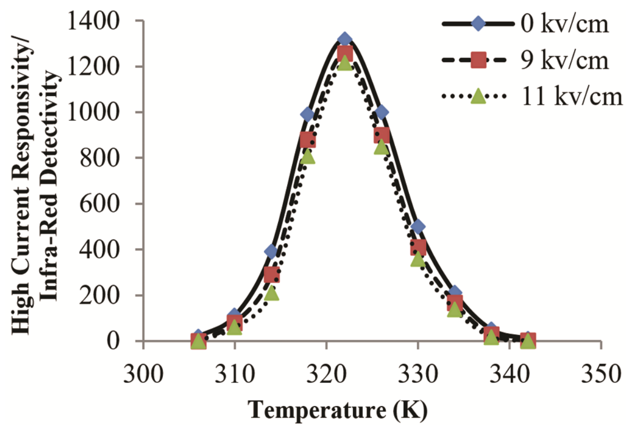

Fig. 4 — Temperature- and electric-field-dependent ratio of High Current Responsivity to Infra-Red Detectivity in $SnCl_2.2H_2O$-TGS crystal, in agreement with the reported experimental data[33]

electron emitting surfaces capable of releasing a substantial fraction of the intrinsic surface charge density, typically on the order of 10^{14} charges per square centimeter. Previous studies have demonstrated high density electron emission reaching energies of approximately 25 keV during slow phase transitions, even in the absence of an external electric field. Considerably higher emission densities and electron energies are expected when fast phase transitions or rapid polarization reversal mechanisms are employed, wherein nearly 10^{10} electrons can be emitted by illuminating the surface of a pre-poled ferroelectric specimen with pulsed laser radiation.

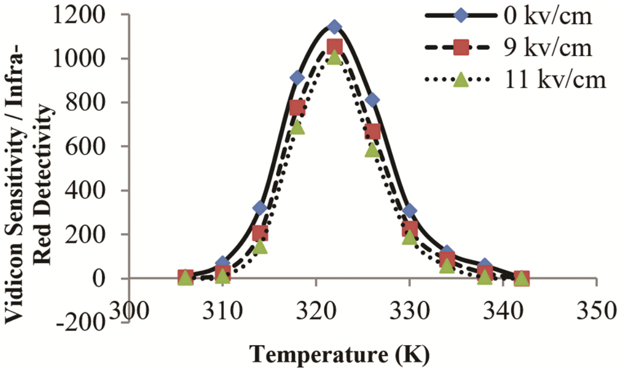

Fig. 5 — Temperature- and electric-field-dependent ratio of Vidicon Sensitivity to Infra-Red Detectivity in $SnCl_2.2H_2O$-TGS crystal, in agreement with the reported experimental data[33]

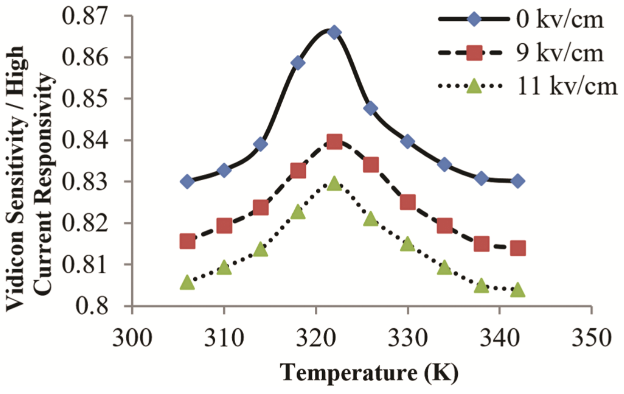

Fig. 6 — Temperature- and electric-field-dependent ratio of Vidicon Sensitivity to High Current Responsivity in $SnCl_2.2H_2O$-TGS crystal, in agreement with the reported experimental data[33]

Figure 4 shows the temperature dependence of the ratio of high current responsivity to infrared detectivity (M_2/M_1) for stannous chloride dihydrate doped triglycine sulphate crystals in the temperature range 300–346 K under external bias fields of 0, 9 and 11 kV cm^{-1}. In the ferroelectric phase below the Curie temperature, the ratio increases gradually with temperature, indicating a progressive enhancement of current responsivity as polarization fluctuations become stronger. Between 300 K and approximately 310 K, the increase in $M_2/M_1$is relatively slow, reflecting stable ferroelectric ordering. As the temperature approaches the Curie temperature, a sharp rise in the ratio is observed, and a maximum value in the range 1200 to 1380 is attained, depending on the applied electric field. This pronounced peak at T_C arises from critical polarization fluctuations and enhanced pyroelectric current generation. Above the Curie temperature, in the paraelectric phase, the ratio decreases with further increase in temperature up to 346 K due to the loss of long-range ferroelectric order. The application of an external electric field significantly varyes (M_2/M_1) throughout the entire temperature range, with the calculated values observed for 11 kV cm^{-1}, indicating strong field-assisted carrier drift and reduced recombination losses. The theoretically evaluated enhancement of the M_2/M_1 ratio in the vicinity of the Curie temperature, as well as its systematic increase under applied electric fields, shows very good quantitative agreement with the experimentally reported trends[33], thereby confirming the validity of the PLCM approach in describing bias-assisted infrared response in $SnCl_2.2H_2O$-doped TGS crystals.

Figure 5 illustrates the variation of the ratio of vidicon sensitivity to infrared detectivity (M_3/M_1) as a function of temperature in the same range of 300–346 K. Below the Curie temperature, M_3/M_1 shows a gradual increase with temperature, reflecting improved optical modulation efficiency as the crystal approaches the phase transition. Near the Curie temperature, the ratio exhibits a distinct maximum, with peak values lying in the range 1000–1190, depending on the magnitude of the applied bias field. This maximum is associated with enhanced coupling between optical excitation and polarization dynamics near T_C. Beyond the Curie temperature, the ratio decreases with increasing temperature due to the transition to the paraelectric phase and the reduction in polarization-related contributions. The applied electric field varyes M_3/M_1 across the entire temperature range, with the calculated values at 11 kV cm^{-1}, demonstrating the effectiveness of external biasing in improving vidicon sensitivity in $SnCl_2.2H_2O$-doped TGS crystals. The magnitude and temperature position of the peak observed in the calculated M_3/M_1 ratio closely correspond to the experimental values reported[33], indicating that the present theoretical model reliably captures the bias-induced enhancement of vidicon sensitivity near the ferroelectric phase transition.

Figure 6 depicts the temperature dependence of the ratio of vidicon sensitivity to high current responsivity (M_3/M_2) shows variation narrow range of 0.83–0.8608 for different bias fields. Unlike the pronounced variations observed in Figs 4 and 5, this ratio exhibits only a weak temperature dependence. Below the Curie temperature, M_3/M_2 increases slightly with temperature and reaches a value close to maximum near T_C. A shallow maximum is observed around the Curie temperature, after which the ratio shows a marginal decrease or saturation above Tc, remaining within the narrow range with unbiased to biased condition. The influence of the applied electric field on this ratio indicates that vidicon sensitivity and current responsivity scale proportionally with both temperature and bias, preserving their relative balance across the ferroelectric paraelectric transition. The temperature and field dependence of the theoretically obtained ratio M_3/M_2 is in excellent conformity with the experimental observations[33], demonstrating that the proportional scaling between vidicon sensitivity and current responsivity is well reproduced within the PLCM framework.

Overall, the temperature-dependent behavior of all three ratios clearly demonstrates that maximum detector performance is achieved near the Curie temperature, where critical polarization fluctuations dominate. Below T_C, the gradual increase in response parameters reflects the strengthening of ferroelectric order, while above T_C , the decrease is attributed to the disappearance of long-range polarization. The systematic enhancement of all response parameters with increasing electric field confirms the crucial role of external biasing in optimizing infrared and vidicon detector performance in $SnCl_2.2H_2O$-doped triglycine sulphate crystals. The close quantitative agreement between the theoretical predictions of the pseudospin–lattice coupled mode model and the experimentally observed trends further validates the applicability of the model to biased ferroelectric detector systems.

The theoretical trends and numerical magnitudes obtained in the present work are in good agreement with the experimental observations[33]. Although he derived their results from direct experimental measurements; the present theoretical values of M_2/M_1, M_3/M_1, and M_3/M_2 follow similar temperature-dependent behavior and fall within the experimentally observed ranges. Minor deviations can be attributed to idealized assumptions in the theoretical model and the absence of microstructural defects and electrode effects. This close correspondence validates the theoretical approach and confirms its usefulness for predicting infrared detection and vidicon performance of $SnCl_2.2H_2O$

doped TGS crystals under practical operating conditions. These characteristics underline the wide applicability of ferroelectric materials in photovoltaic devices, optical sensors, and related technologies. In the present work, stannous chloride dihydrate doped triglycine sulphate (TGS) crystals have been modelled as a coupled harmonic and anharmonic pseudospin lattice vibrational system. The Hamiltonian was formulated under finite probability polarization constraints, and the infrared responsivity, high current responsivity, and vidicon sensitivity of the doped TGS crystal were evaluated. The results reveal that the corresponding figure of merit ratios exhibit pronounced maxima at the Curie temperature and decrease progressively with increasing external electric field, which also induces a slight downward shift in the Curie point. These observations suggest that stannous chloride dihydrate doped TGS crystals are strong materials for applications in photo detection and related optoelectronic technologies. Furthermore, the theoretical framework developed herein is sufficiently general to be extended to other pseudospin-vibrational ferroelectric systems, including KDP-TGS, $MgCl_2$-TGS, ADP-TGS, Rochelle salt, Tin chloride crystal and their dopped crystal forms.

6 Conclusion

The present PLCM framework generally treats the Ising pseudospins within a mean-field or decoupling approximation. Future work may incorporate quantum fluctuations more rigorously by using higher-order Green's function decoupling schemes, Introducing transverse-field corrections explicitly in the Hamiltonian. This would improve the description of tunneling effects near and above Tc, especially for doped TGS where disorder enhances quantum effects.

The PLCM framework combined with the Ising pseudospin model provides a robust description of $SnCl_2.2H_2O$–TGS; however, its predictive power can be significantly enhanced by incorporating quantum fluctuations, dopant-induced disorder, nonlinear coupling, and non-equilibrium effects, which remain promising directions for future research.

Reference

1 Mathias B T, Miller C E & Remeika J P, *Phys Rev*, 104 (1956) 849.

2 Novotný J, Podvalová Z & Zelinka J, *Crystal Growth & Design*, 3 (3) (2003) 393.

3 Eng L M, Bammerlin M, Loppacher Ch, Guggisberg M, Bennewitz R, Meyer E & Güntherodt H J, *Surf Interface Anal*, 27 (1999) 422.

4 Chaudhuri B K, Choudhury K R & Banerjee S, *Phys Rev B*, 38 (1988) 689.

5 Gonzalo J A, *Phys Rev B*, 1 (1970) 3125.

6 Zubarev D N, *Sov Phys Usp*, 3 (1960) 320.

7 Upadhyay T C, Kumar P & Nautiyal A, *Afr Rev Phys*, 7 (2012) 57.

8 Shaheen A, Aljarrah M, Etier M, El-Sheikh A H & Salman F, *Jordan J Phys*, 15 (4) (2022) 369.

9 Manoharan A J J, John N J, Revathi V, Rajendran K V & Andavan P M, *Indian J Sci Technol*, 4 (6) (2011) 688.

10 Kumar R, Kumar B & Singh N, *Mater Sci Eng B*, 313 (2025) 117977.

11 Ramesh S, Anandan P & Jayavel R, *Indian J Pure Appl Phys*, 56 (2018) 721.

12 Iwasaki K, Fujii S, Tanaka H & Morita Y, *J Electron Mater*, 53 (2024) 2154.

13 Kumar A & Verma R, *Indian J Pure Appl Phys*, 59 (2021) 489.

14 Mousa E, Hassan A & El-Mallah H, *Phys Scr*, 99 (2024) 095702.

15 Merz W J, *Phys Rev*, 95 (1954) 690.

16 Handerek J, Pisarski M & Ujma Z, *J Phys C: Solid State Phys*, 14 (1981) 2007.

17 Sujak B & Sysło W A, *Ferroelectrics*, 22 (1978) 711.

18 Biedrzycki K, *Phys Status Solid (a)*, 109 (1) (1988) 11–364, K79.

19 Peercy P S, *Phys Rev B*, 13 (1976) 3945.

20 Samara G A, *Ferroelectrics*, 20 (1978) 87.

21 Kobayashi K, *J Phys Soc Jpn*, 24 (1968) 297.

22 Mitsui T, *Phys Rev*, 111 (1958) 1259.

23 Nettleton R E, *J Phys C: Solid State Phys*, 8 (1975) 943.

24 Blinc R, Arend H & Kanduser A, *Phys Status Solid (b)*, 74 (1976) 425.

25 Mavroyannis C & Pathak K N, *Phys Rev*, 182 (1969) 872.

26 Born M & Huang K, *Dynamical Theory of Crystal Lattices*, Oxford University Press, New York (1954) 1.

27 Semwal B S & Sharma P K, *Prog Theor Phys*, 51 (1974) 693.

28 Upadhyay T C, Panwar N S & Semwal B S, *Int J Mod Phys B*, 9 (1995) 45.

29 Upadhyay T C & Semwal B S, *Indian J Pure Appl Phys*, 40 (2002) 615.

30 Upadhyay T C & Semwal B S, *Pramana J Phys*, 60 (2003) 525.

31 Upadhyay T C, Singh R & Semwal B S, *Pramana J Phys*, 67 (2006) 547.

32 Semwal B S & Sharma P K, *Phys Rev B*, 5 (1972) 3909.

33 Banan B, Lal R B & Batra A, *J Mater Sci*, 27 (1992) 2291.